Binder-Free Two-Dimensional Few-Layer Titanium Carbide MXene Ink For High-Performance Symmetric Supercapacitor Device Applications

Vediyappan Thirumal, Palanisamy Rajkumar, Jin-Ho Kim*, Bathula Babu* and Kisoo Yoo*

Department of Mechanical Engineering, Yeungnam University, Gyeongsan-si 38541, Gyeongsangbuk-do, Republic of Korea; thirumalvisnu@gmail.com (V.T.); rajphysics@yahoo.com (P.R.)

* Correspondence: jinho@ynu.ac.kr (J.-H.K.); babu.physicist@gmail.com (B.B.); kisooyoo@ynu.ac.kr (K.Y.)

Supporting information (SI)

After Cycling stability of MXene-ink symmetry electrode FE-SEM surface morphology.

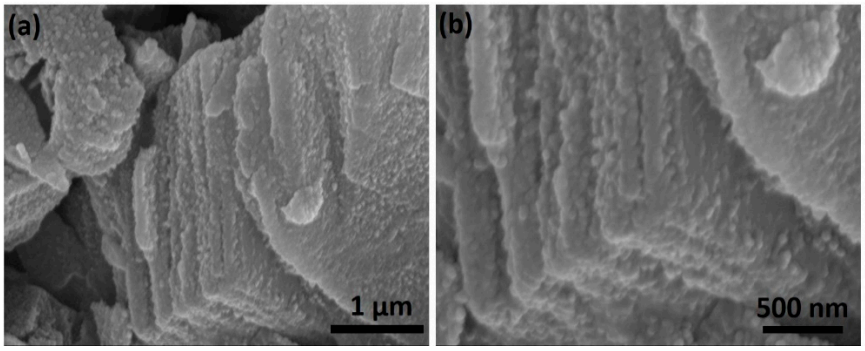

Figure S1. Surface morphology images of MXene-ink for after 10,000 cycling FE-SEM images.

Figure S1 Electrode morphology change after cycling surface imaging of MXene reveals notable slighly changes, after long charge-discharge cycles indicating the impact of electrochemical processes. After cycling, SEM analysis of MXene ink reveals subtle changes in surface morphology. Despite extended cycling, the alterations observed are minimal, suggesting the robustness of MXene-based electrodes. These slight changes may indicate minor structural reorganization or surface modifications over long cycles, indicative of MXene's stability under repeated electrochemical processes. Such consistent morphology

even after prolonged cycling underscores the potential of MXene inks for durable energy storage applications, promising long-term performance and reliability in various electrochemical devices.

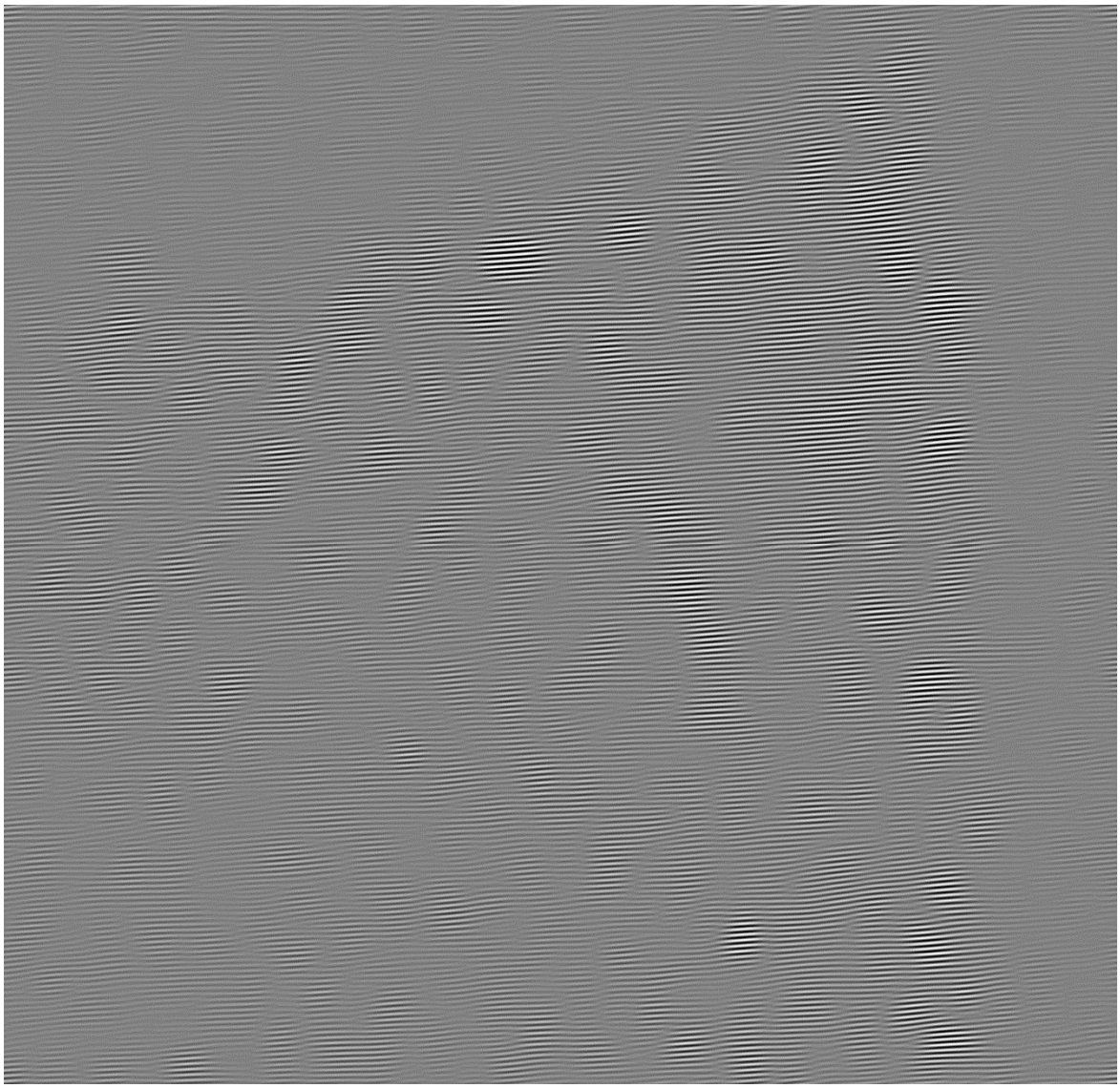

Figure S2. Inverse Fast Fourier Transform (IFFT) fringe images of magnified view (original source from MXene-ink HR-TEM images).

XPS Analysis (MXene ink)

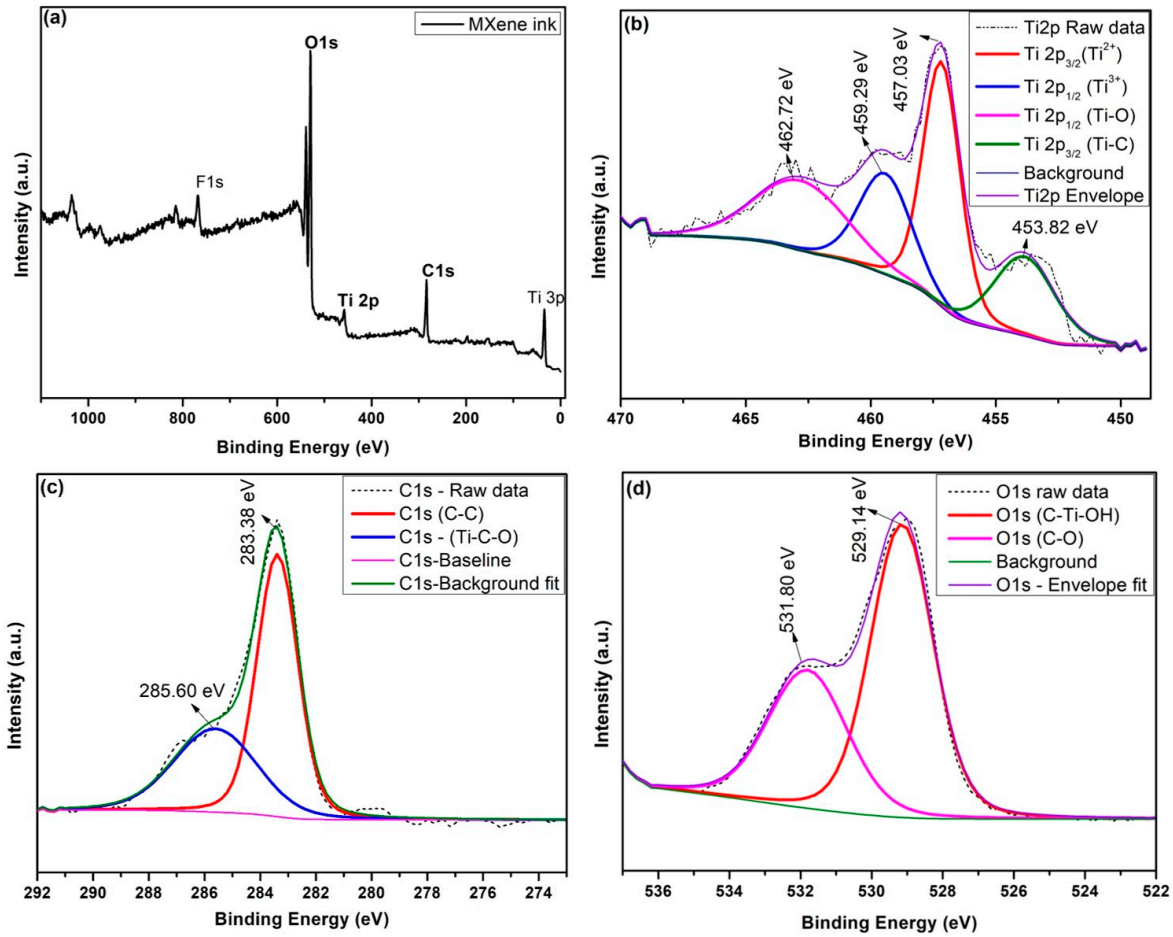

Figure S3. (a) XPS survey of MXene-ink sample, de-convoluted XPS spectra of (b) Ti2p, (c) C1s, and (d) O1s.

Figure S3(a) depicts the appearance of the survey spectrum showing peaks from C1s, Ti 2p (Ti 2p1/2 & 2p3/2), and O1s at assigned binding energy values of 283.90 eV, 457.17 eV and 529.14 eV, respectively. Additionally, supplementary binding energy peaks at 33.83 eV and 760.15 eV for elements Ti 3p and F1s indicate the presence of functional groups, revealing insights into the wet-chemical etching process. Figure 3a–d displays a series of high-resolution XPS spectra. The Ti 2p spectrum (Figure S3(b)) was fitted with four doublets (Ti 2p3/2 and Ti 2p1/2). The binding energies of the three prominent peaks were further deconvoluted into Ti 2p3/2 & 2p1/2 for Ti−C, Ti^{2+}, Ti^{3+}, and Ti−O, yielding values of 453.82, 457.03, 459.29, and 462.72 eV, respectively. Subsequently, Figure S3(b) Ti 2p3/2 and Ti 2p1/2) corresponds assigned bonding for Ti-C and Ti-O peaks respectively. The distinctive

components of the Ti-C bonding energy reveal distinct components corresponding to Ti(3+), owing to the spin–orbit splitting of 2p into 2p3/2 and 2p1/2 [1]. In Figure S3(c), the C1s spectrum in Fig. S3(c) was deconvoluted into four peaks centered at 283.38 eV and 285.60 eV, corresponding to C-C and Ti-C-O, respectively. The O1s spectrum showed significant differences from oxidized MXene, with peaks in Figure S3(d) de-convoluted into four peaks centered at 530.9, 531.7, 532.6, and 533.6 eV, corresponding to surface species of C−Ti−OH, C−O, adsorbed oxygen, and surface terminal hydroxyl groups, respectively [2]. This finding confirms the presence of functional groups on the surface of the $Ti_3C_2T_x$ ink, validating the XPS results.

Bare-Ni-foam studies

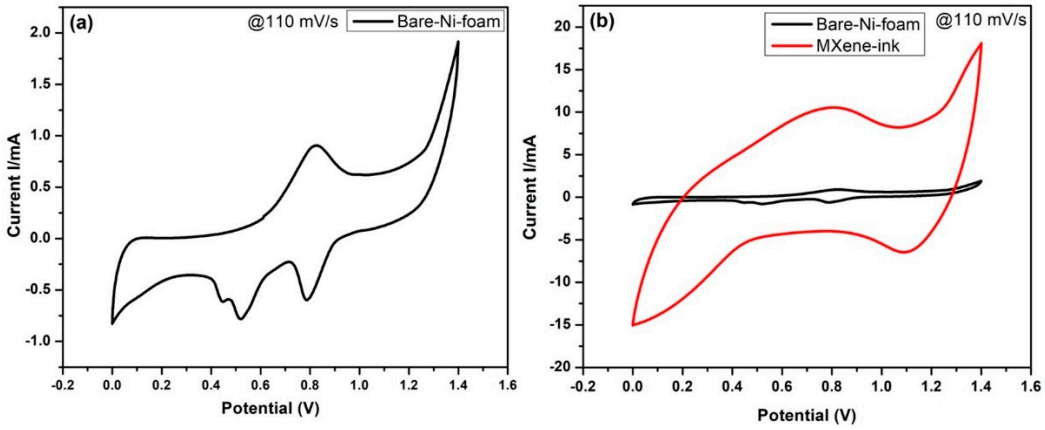

Figure S4. (a) CV of the bare Ni foam (current collector substrate) and (b) comparative bare Ni-foam with the as-prepared MXene-ink electrodes at a fixed scan rate of 100 mV/s in 3 M KOH aqueous electrolyte.

Figure S4 (a) CV curves scan rate at 110 mV/s, its reveals that the bare nickel foam substrate exhibits oxidation/reduction redox pseudo-capacitive behavior due to its inherent surface properties. This behavior is attributed to the presence of active sites on the nickel foam surface, which facilitate reversible redox reactions due to their metallic active surface may provide the redox behavior. Figure S4 (b) Hence, here compared with MXene ink coated Ni-foam, when compared to slurry-coated Ni-foam, the bare nickel foam substrate typically

demonstrates at same scan rates at 110 mV/s, accordingly clearly shows the bare and MX-ink coated electrodes enhanced electrochemical CV curve area with the redox pseudocapacitive behavior, possibly due to the direct exposure good binding Mxene layers by layer interference.

MAX (Ti_3AlC_2) symmetric device Analysis

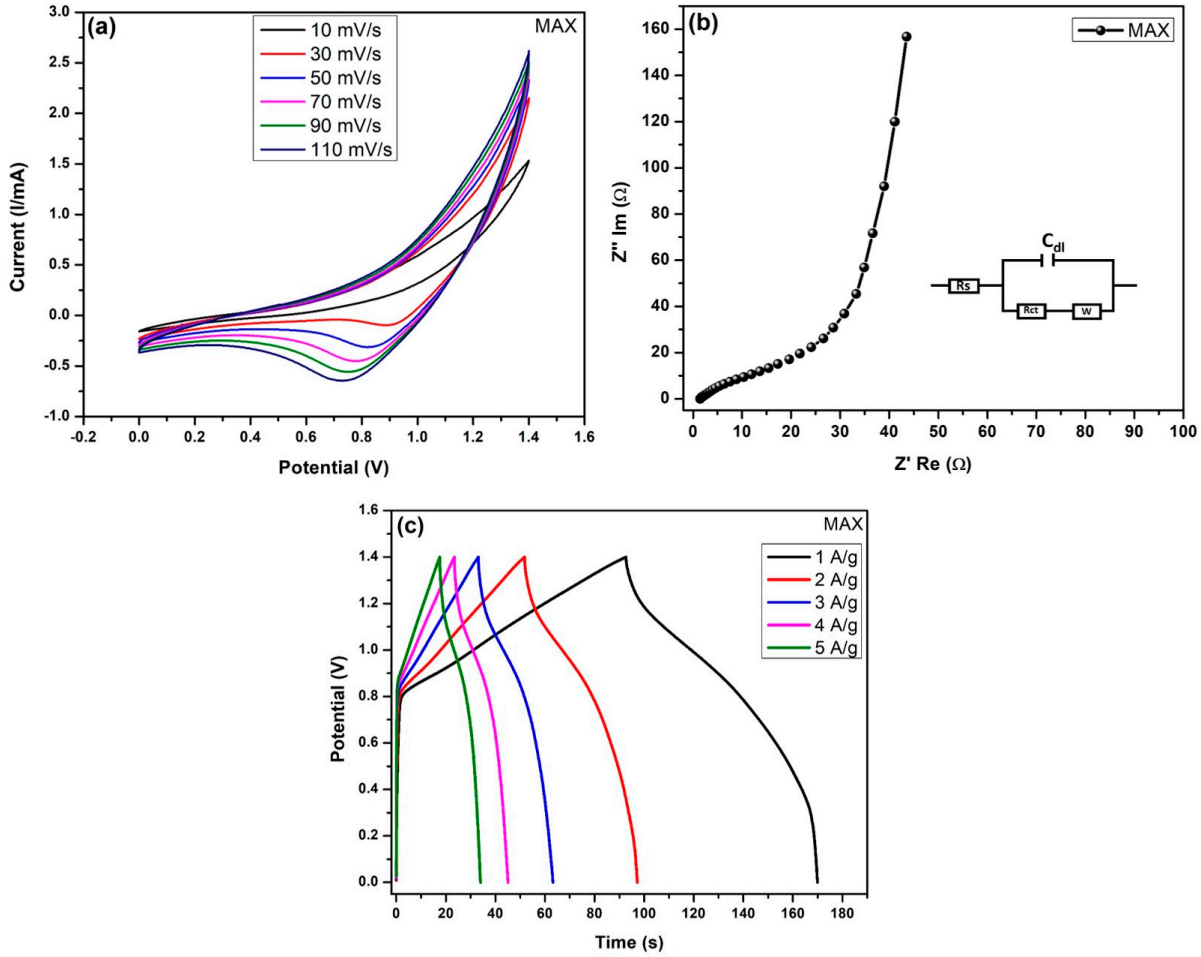

Figure S5. (a) CV curves with various scan rate for the MAX (Ti_3AlC_2) symmetric device with different scan rate. (b) EIS Nyquist plot with Randel circuit (inset) and (c) charge-discharge curves current densities in symmetric device.

Cyclic Voltammetry (CV): The CV analysis of the MAX phase symmetry supercapacitor exhibited wothout-defined reduction peaks, indicative of MAX (Ti_3AlC_2) phase precursor less efficient charge storage and ionic intercalation. Figure S5 (a) shows the cyclic

voltammetry profiles of MAX collected at potential scan rates from 10 to 110 mV/s in the potential range 0−1.4V potential window with 1 M KOH aqueous solution. While increasing the scan rates from 10−110mV/s further cycles may not result in additional redox peaks due to saturation of these active sites, as further oxidation or reduction processes become limited. Figure S5 (b) display the electrochemical impedance spectroscopy (EIS) measurements revealed low charge transfer resistance and Warburg impedance, indicative of fast ion diffusion and favorable charge transport within the electrode-electrolyte interface. In addition, (EIS) analysis using Randels circuit model reveals key parameters: Rs (solution resistance), Rct (charge transfer resistance), and W (Warburg impedance). From the nyquest plot the resistance to charge transfer at the Rct – 28.7Ω. The observed Nyquist plot demonstrated a semicircle at high frequencies followed by a linear region at low frequencies, consistent with the ideal behavior of a capacitive system for assessing electrochemical kinetics.

The electrochemical properties of galvanostatic charge-discharge (GCD) profiles exhibited symmetric charge-discharge curves indicating tri-angle curves shown in Figure S5 (d). The nearly linear discharge behavior reflects the capacitive nature of the MAX (Ti_3AlC_2) electrode material, highlighting its suitability for rapid energy storage and delivery in symmetric supercapacitor devices. The MAX (Ti_3AlC_2) symmetric device current density (A/g) of 1 A/g, 2 A/g, 3 A/g, 4 A/g, 5 A/g corresponds to the specific capacitance (Csp) 49.29 F/g, 34.53 F/g, 22.60 F/g, 16.80 F/g, 12.95 F/g, respectively. These CV, EIS and GCD results demonstrate the practical electrochemical performance of MAX phase symmetry supercapacitors.

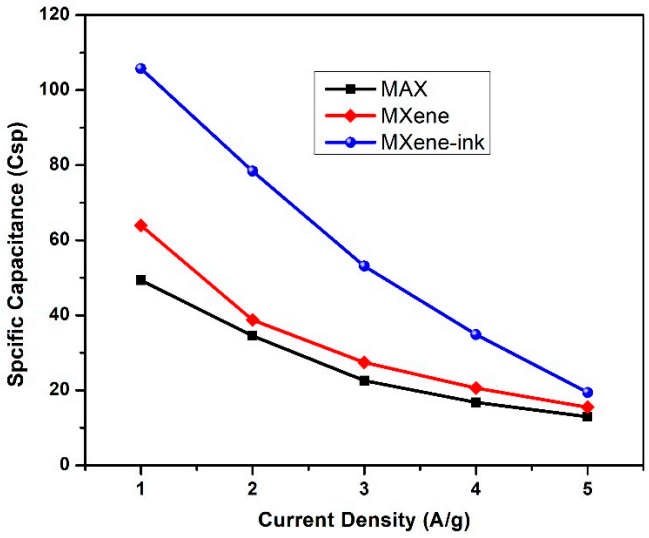

Figure S6. Relationship between specific capacitance (Csp) versus current densities (A/g) for all electrodes.

Table S1. Z-fit analysis results for MXene-ink symmetric device: relative parameters relative error with stop fit at $1\times e^{-3}$, and Weight: $|Z|^2$

Equivalent circuit: R1+C1/(R2+W1) Standard value	Standard error
R1 = 1.4161758 Ohm	std err. R1 = 0.0874224 Ohm
C2 = 0.00012920 F	std err. C2 = 23.6741504 e^{-6} F
R2 = 9.7014170 Ohm	std err. R2 = 0.2167858 Ohm
W1 = 36.0714864 Ohm.$s^{-1/2}$	std err. W1 = 3.0587993 Ohm.$s^{-1/2}$
$Chi^2/|Z|^2$ = 0.6695639	Chi / sqrt(N) = 6.237275787 Ohm

Table S2. Z-fit analysis for MXene symmetric device.

Equivalent circuit: R1+C1/(R2+W1) Standard value	Standard error
R1 = 0.5029445 Ohm	std err. R1 = 0.0267670 Ohm
C2 = 0.0011619 F	C2 = 48.9186307e^{-6} F
R2 = 10.7139048 Ohm	std err. R2 = 22.4740343 Ohm
W1 = 55.8644823 Ohm.$s^{-1/2}$	std err. W1 = 15.4870929 Ohm.$s^{-1/2}$
$Chi^2/|Z|^2$ = 0.6509440	Chi / sqrt(N) = 20.2670127 Ohm

Table S3. Comparison of MXene with metallic nanocomposite supercapacitor different electrode.

S.No	Materials/applications	Method of preparation	Electrolyte	Specific capacitance	Ref.
1.	MXene ink (printing micro-supercapacitor)	NMP + $Ti_3C_2T_x$ Inkjet printing	3 M H_2SO_4 + PVA) gel electrolyte	562 $F.cm^{-3}$ @ 20 $\mu A.cm^{-2}$	[3]
2.	2. Graphene ink	inkjet printing with dry etching	PVA/H_3PO_4 electrolyte	99 $\mu F.cm^{-2}$ @ 0.025 $\mu A.cm^{-2}$	[4]
3.	3D-printed AC/CNT/MXene-N/GO ink (symmetric Supercapacitor)	melamine formaldehyde (MF) template (photochemigraphy) method	3 M H_2SO_4 + PVA) gel electrolyte	8.2 $F.cm^{-2}$ 0.025 $\mu A.cm^{-2}$	[5]
4.	$Ti_3C_2T_x$/CMC/CNT membrane electrode for asymmetric micro-supercapacitors	Etching LiF/HCl MXene-film synthesized by vacuum filtration	1M H_2SO_4 electrolyte.	1431.4 $mF.cm^{-2}$ @1 $mA.cm^{-2}$)	[6]
5.	Ti_3C_2/CuS//Ti_3C_2 asymmetric supercapacitors	hydrothermally CuS + Ti_3C_2 sheets selectively etching Ti_3AlC_2,	1 M KOH	49.3 Fg^{-1}@ 1 Ag^{-1}	[7]
6.	d-Ti_3C_2/NF//d-Ti_3C_2 supercapacitor	3D Ni foam by electrostatic self-assembly.	6 M KOH	51.1 Fg^{-1}@0.5 Ag^{-1}	[8]
7.	3-dimentional MXene/NCF//MXene/NCF supercapacitor	(3D) interconnected neuron-like directly prepared by one-step pyrolysis method	PVA/KOH	63 Fg^{-1}@ 1 Ag^{-1}	[9]
8.	rGO//$Ti_3C_2T_x$	rGO/MXene hydrogel films	3 M H_2SO_4	76.5 Fg^{-1}@1 Ag^{-1}	[10]
9.	rGO//$Ti_3C_2T_x$/CoS_2 supercapacitor	CoS_2 on MXene surface by a simple one-step solvent thermal method	2 M KOH	80.6 Fg^{-1}@1 Ag^{-1}	[11]
10.	**$Ti_3C_2T_x$ // $Ti_3C_2T_x$ MXene ink (symmetric device)**	**Facile Sonication and high centrifuge technique**	**3 M KOH**	**105.75 F/g @1A/g**	**This work**

References

1. Chen, W.Y.; Jiang, X.; Lai, S.N.; Peroulis, D.; Stanciu, L.; Nanohybrids of a MXene and transition metal dichalcogenide for selective detection of volatile organic compounds. *Nature communications* **2020**, 11, 1302. https://doi.org/10.1038/s41467-020-15092-4.
2. Yin, Z.; Lu, Z.; Xu, Y.; Zhang, Y.; He, L.; Li, P.; Xiong, L.; Ding, L.; Wei, Y.; Wang, H. Supported MXene/GO Composite Membranes with Suppressed Swelling for Metal Ion Sieving. *Membranes* **2021**, 11, 621. https://doi.org/10.3390/membranes11080621.
3. Zhang, C.; McKeon, L.; Kremer, M.P.; Park, S.-H.; Ronan, O.; Seral-Ascaso, A.; Barwich, S.; Coileáin, C.; McEvoy, N.; Nerl, H.C.; et al. Additive-free MXene inks and direct printing of micro-supercapacitors, *Nat. Commun.* **2019**, *10*, 1795.
4. Delekta, S.S.; Smith, A.D.; Li, J.; Östling, M. Inkjet printed highly transparent and flexible graphene micro-supercapacitors. *Nanoscale*, **2017**, 21, 6998-7005. https://doi.org/10.1039/C7NR02204B.
5. Yu, L.; Fan, Z.; Shao, Y.; Tian, Z.; Sun, J.; Liu, Z. Versatile N-doped MXene ink for printed electrochemical energy storage application. *Adv. Energy Mater.* **2019**, *9*, 1901839.

6. Xu, H.; Zhu, J.; Xu, M.; Lei, Z.; Hu, Q.; Jin, X. Flexible and alternately layered high electrochemical active electrode based on MXene, carboxymethylcellulose, and carbon nanotube for asymmetric micro-supercapacitors. *Journal of Colloid and Interface Science*, **2023**, 645, 974–984.
7. Pan, Z.; Cao, F.; Hu, X.; Ji, X. A facile method for synthesizing CuS decorated Ti 3 C 2 MXene with enhanced performance for asymmetric supercapacitors. *Journal of Materials Chemistry A*. **2019**, 7, 8984– 8992. https://doi.org/10.1039/C9TA00085B.
8. Guo, J.; Zhao, Y.; Ma, T. Electrostatic self-assembly of 2D delaminated MXene (Ti3C2) onto Ni foam with superior electrochemical performance for supercapacitor. *Electrochimica Acta*. **2019**, 305, 164–174, https://10.1016/j.electacta.2019.03.025.
9. Sun, L.; Song, G.; Sun, Y.; Fu, Q.; Pan, C. MXene/N-Doped Carbon Foam with Three-Dimensional Hollow Neuron-like Architecture for Freestanding, Highly Compressible All Solid-State Supercapacitors. *ACS Appl. Mater. Interfaces* **2020**, 12, 44777– 44788. https://10.1021/acsami.0c13059.
10. Wang, S.; Zhao, X.; Yan, X.; Xiao, Z.; Liu, C.; Zhang, Y.; Yang, X. Regulating Fast Anionic Redox for High-Voltage Aqueous Hydrogen-Ion-based Energy Storage. *Angew. Chem*. **2019**, 131, 211–216. https://10.1002/ange.201811220.
11. Liu, H.; Hu, R.; Qi, J.; Sui, Y.; He, Y.; Meng, Q.; Wei, F.; Ren, Y.; Zhao, Y.; Wei, W. One-Step Synthesis of Nanostructured CoS2 Grown on Titanium Carbide MXene for High-Performance Asymmetrical Supercapacitors. *Adv. Mater. Interfaces* **2020**, 7, 1901659. https://10.1002/admi.201901659.